Available online at www.sciencedirect.com
ScienceDirect
Fluid Phase Equilibria 260 (2007) 300–315
FLUID PHASE EQUILIBRIA
www.elsevier.com/locate/fluid

Modelling of calcium sulphate solubility in concentrated multi-component sulphate solutions

G. Azimi [a], V.G. Papangelakis [a,*], J.E. Dutrizac [b]

[a] *Department of Chemical Engineering and Applied Chemistry, University of Toronto, Toronto, Ontario M5S 3E5, Canada*
[b] *CANMET, Natural Resources Canada, 555 Booth Street, Ottawa, Ontario K1A 0G1, Canada*

Received 16 January 2007; received in revised form 18 May 2007; accepted 19 July 2007
Available online 2 August 2007

Abstract

The chemistry of several calcium sulphate systems was successfully modelled in multi-component acid-containing sulphate solutions using the mixed solvent electrolyte (MSE) model for calculating the mean activity coefficients of the electrolyte species. The modelling involved the fitting of binary mean activity, heat capacity and solubility data, as well as ternary solubility data. The developed model was shown to accurately predict the solubility of calcium sulphate from 25 to 95 °C in simulated zinc sulphate processing solutions containing $MgSO_4$, $MnSO_4$, $Fe_2(SO_4)_3$, Na_2SO_4, $(NH_4)_2SO_4$ and H_2SO_4. The addition of H_2SO_4 results in a significant increase in the calcium sulphate solubility compared to that in water. By increasing the acid concentration, gypsum, which is a metastable phase above 40 °C, dehydrates to anhydrite, and the conversion results in a decrease in the solubility of calcium sulphate. In $ZnSO_4$–H_2SO_4 solutions, it was found that increasing $MgSO_4$, Na_2SO_4, $Fe_2(SO_4)_3$ and $(NH_4)_2SO_4$ concentrations do not have a pronounced effect on the solubility of calcium sulphate. From a practical perspective, the model is valuable tool for assessing calcium sulphate solubilities over abroad temperature range and for dilute to concentrated multi-component solutions.

Keywords: Calcium sulphate; Gypsum; Anhydrite; Zinc hydrometallurgy; Solubility; Chemical modelling; OLI; Hydrometallurgy

1. Introduction

Calcium sulphate occurs in three forms: dihydrate (or gypsum) (DH: $CaSO_4{\cdot}2H_2O$), hemihydrate (or bassanite) (HH: $CaSO_4{\cdot}0.5H_2O$) and anhydrite (AH: $CaSO_4$), depending on the temperature, pH and formation conditions. Calcium sulphate occurs widely in nature as gypsum and anhydrite, and is encountered in many industrial processes such as the evaporation of brines and the manufacture of phosphate fertilizer. Calcium sulphate commonly precipitates during the neutralization of free sulphuric acid or in iron removal operations where sulphates are eliminated from aqueous solutions by the addition of calcium-containing bases such as lime or limestone. Because of its relative insolubility, calcium sulphate is deposited almost everywhere calcium and sulphate occur together in aqueous solutions. The resulting scales are a major concern because they form even at low pH and can be effectively removed only by mechanical means. A recent evaluation of one process estimated that the control of calcium sulphate in that operation alone cost between $6 and $10 million per year [1].

Many studies have attempted to theoretically model the solubilities of the calcium sulphate compounds in water and in multi-component aqueous solutions. The solubility of calcium sulphate hydrates is equal to the sum of the molalities of the free calcium ion, Ca^{2+}, and the associated calcium sulphate neutral species, $CaSO_{4(aq)}$. Consequently, the solubility of calcium sulphate hydrates is governed by the following equilibria:

$$CaSO_4{\cdot}nH_2O(S) \leftrightarrow Ca^{2+} + {SO_4}^{2-} + nH_2O \quad (1)$$

$$Ca^{2+} + {SO_4}^{2-} \leftrightarrow CaSO_{4(aq)} \quad (2)$$

where $n = 0$, 0.5 and 2 corresponding to anhydrite, hemihydrate and dihydrate, respectively. The thermodynamic equilibrium constants for reactions (1) and (2) are:

$$K^0_{SP} = (m_{ca^{2+}}\gamma_{ca^{2+}})(m_{SO_4^{2-}}\gamma_{SO_4^{2-}})(a_{water})^n$$
$$= (m_{ca^{2+}})(m_{SO_4^{2-}})\gamma^2_{\pm(CaSO_4)}(a_{water})^n \quad (3)$$

* Corresponding author.
E-mail address: papange@chem-eng.utoronto.ca (V.G. Papangelakis).

0378-3812/$ – see front matter © 2007 Elsevier B.V. All rights reserved.
doi:10.1016/j.fluid.2007.07.069

$$K_a = \frac{a_{CaSO_4}}{a_{Ca^{2+}} a_{SO_4^{2-}}} \quad (4)$$

The solubility of calcium sulphate is:

$$[Ca]_{total} = m_{Ca^{2+}} + m_{CaSO_{4(aq)}} \quad (5)$$

where K^0_{SP} is the solubility product, K_a the association constant of calcium sulphate neutral species, m molality (mol kg^{-1}), $\gamma_{\pm(CaSO_4)}$ the mean activity coefficient of $CaSO_4$, $\gamma_{CaSO_{4(aq)}}$ the activity coefficient of calcium sulphate neutral species and a_{water} is the activity of water. To calculate the solubility of calcium sulphate hydrates, all the above need to be determined.

Marshall and Slusher [2], Tanji and Doneen [3], Zemaitis et al. [4], Demopoulos et al. [5] and Arslan and Dutt [6] proposed different methods based on different correlations for the activity coefficient that include the extended Debye–Hückel and Guggenheim–Davies expressions, as well as the Bromley, Meissner or Pitzer models to predict the solubility of calcium sulphate in various electrolyte solutions.

More recently, Adams [1] studied gypsum scale formation in a continuous sulphuric acid neutralization process. In this work, the solubility of gypsum and its scaling potential in sulphate systems were accurately modelled with the aid of the OLI software package (http://www.olisystems.com) using the mixed solvent electrolyte (MSE) [7–9] activity coefficient model for the temperature range from 25 to 90 °C. This model was capable of predicting the gypsum solubility over the indicated temperature range. However, other forms of calcium sulphate; i.e., anhydrite and hemihydrate were not taken into account in this study.

Li and Demopoulos [10] recently developed a model for the solubility of calcium sulphate in multi-component aqueous chloride solutions over the temperature range from 10 to 100 °C. The Bromley–Zemaitis activity coefficient model [11] was used, and the regression of the experimental data was carried out with the aid of the OLI software package.

Most of the previous studies focused on the solubility of gypsum at temperatures below 100 °C. Although mixed multi-component systems of sulphates are present in neutralization reactors, zinc processing solutions and pressure acid leaching circuits, no previous work had been formally undertaken to study the solubility of the three phases of calcium sulphate in such solutions. In particular, little work has been reported over a wide temperature range, and no phase transition diagram has been established among the different calcium sulphate hydrates in such complex mixed aqueous electrolytes.

In this work, the solubility of calcium sulphate systems was successfully modelled using the mixed solvent electrolyte (MSE) model [7–9]. The modelling involved the regression of binary activity, heat capacity and solubility data, as well as ternary solubility data. New interaction parameters for free calcium ions and associated calcium sulphate neutral species with other dominant species in the solution were also determined. The procedures followed were similar to those described elsewhere [12].

2. Chemical modelling

2.1. Equilibrium constant

To obtain the equilibrium constants in Eqs. (3) and (4) at temperature T and pressure P, the standard state chemical potentials of the products and reactants must be known. These data are widely available in standard thermodynamic compilations. The *HKF model*, developed by Tanger and Helgeson [13], is embedded in the OLI software to calculate the standard state thermodynamic properties at high temperatures and pressures, up to 1000 °C and 5 kbar. The general equation is as follows:

$$X^0_{T,P} = X(T, P, a_1, a_2, a_3, a_4, c_1, c_2, \bar{\omega}) \quad (6)$$

where X denotes a thermodynamic function such as chemical potential (μ), partial molal enthalpy (H), entropy (S), volume (V), or heat capacity (C_p), and $a_1, a_2, a_3, a_4, c_1, c_2, \bar{\omega}$ are HKF parameters.

2.2. Activity coefficient model

The activity coefficient is a parameter which accounts for the nonideality (excess properties) of electrolyte solutions, and is defined by the excess Gibbs free energy of the solution, G^E:

$$\ln\gamma_i = \left(\frac{\partial(G^E/RT)}{\partial n_i}\right)_{T,P,n_{i\neq j}} \quad (7)$$

where n_i is the number of moles of the solution constituents (species i), and j is any other species. The pursuit of an expression for G^E to calculate γ has been ongoing for decades. Numerous models have been proposed and some of them have been incorporated into commercial software and applied in industry [12].

The more recently developed mixed solvent electrolyte (MSE) model [7–9] is capable of accurately calculating the thermodynamic properties of electrolyte solutions in water and/or organic solvent(s) over the entire concentration range from infinite dilution to pure fused salt electrolytes. The application of the MSE model within the OLI software platform for hydrometallurgical processing solutions has already proved its efficiency and accuracy in predicting the properties of multi-component solutions [12,14].

In this work, the MSE model used in the OLI software platform is employed. In the MSE model, the excess Gibbs free energy consists of three terms [8]:

$$\frac{G^E}{RT} = \frac{G^E_{LR}}{RT} + \frac{G^E_{MR}}{RT} + \frac{G^E_{SR}}{RT} \quad (8)$$

where G^E_{LR} represents the contribution of long-range electrostatic interactions expressed by the Pitzer–Debye–Hückel equation, G^E_{SR} is the short-range contribution term resulting from molecule–molecule, molecule–ion and ion–ion interactions that is calculated by the UNIQUAC model, and G^E_{MR} accounts for the middle-range ionic interactions (i.e., ion–ion, ion–molecule) that are not included in the long-range term. The middle-range

term is a second virial coefficient-type term for the remaining ionic interactions:

$$\frac{G^{E}_{MR}}{RT} = -\left(\sum_i n_i\right)\sum_i\sum_j x_i x_j B_{ij}(I_x) \quad (9)$$

where x is the mole fraction of species, and B_{ij} is a binary interaction parameter between species i and j (ion or molecule) and is similar to the second virial coefficient, which is a function of ionic strength according to the following equations:

$$B_{ij}(I_x) = b_{ij} + c_{ij}\exp(-\sqrt{I_x + 0.01}) \quad (B_{ij} = B_{ji}) \quad (10)$$

$$b_{ij} = \mathrm{BMD0} + \mathrm{BMD1} \times T + \frac{\mathrm{BMD2}}{T} + \mathrm{BMD3} \times T^2 + \mathrm{BMD4} \times \ln T \quad (11)$$

$$c_{ij} = \mathrm{CMD0} + \mathrm{CMD1} \times T + \frac{\mathrm{CMD2}}{T} + \mathrm{CMD3} \times T^2 + \mathrm{CMD4} \times \ln T \quad (12)$$

where BMDk (k=0, ..., 4) and CMDk (k=0, ..., 4) are adjustable parameters between species i and j that can be obtained by the regression of experimental data such as the mean activity coefficient, activity of water, osmotic coefficient, heat capacity and solubility.

The regression parameters in the MSE framework are those of the UNIQUAC and middle-range parameters. UNIQUAC parameters are primarily for neutral-neutral species and middle-range parameters are primarily for ion–ion and ion–neutral species. It has been found that for moderately concentrated single-solvent electrolyte solutions, the UNIQUAC terms are not needed to describe the systems [7,8]. This helps to avoid over-parameterization.

2.3. Standard state Gibbs free energy and entropy

The adjustment of the standard state Gibbs free energy and entropy is the most useful method to determine the optimum solubility product values for solid phases. This can be accomplished by regressing experimental solubility and heat capacity data of the solid phase (if available) at various temperatures.

In this work, the standard state Gibbs free energy and standard state entropy, as well as the heat capacity equation parameters (CPS_i in Eq. (13)) of those solids for which there were not temperature-dependent data in existing thermodynamic compilations (i.e., the OLI software default database) were regressed, using available experimental solubility data.

$$C_p = \mathrm{CPS1} + \mathrm{CPS2} \times T + \frac{\mathrm{CPS3}}{T^2} + \mathrm{CPS4} \times T^2 + \mathrm{CPS5} \times T^3 \quad (13)$$

2.4. Regression of the experimental data

Regression of the experimental data by the same model ensures self-consistency. The validation of the model parameters is made by comparing the model results with the experimental data beyond the range of the available data used to determine the parameters.

2.5. Case studies

Numerous experimental data from various studies are available for the solubility of calcium sulphate hydrates in sulphate solutions. In this study, different binary, ternary, quaternary and more complex multi-component sulphate systems were investigated. The model parameter estimation was performed by regressing the available experimental data in binary and ternary

Table 1
Different systems studied for the chemical modelling of $CaSO_4$ in sulphate solutions

System	Data type	Temperature range (°C)	Solid phases	References
Binary systems				
$MnSO_4$–H_2O	$\gamma_{\pm}$-a_{water}-C_p-solubility	0–180	$MnSO_4{\cdot}7H_2O$, $MnSO_4{\cdot}5H_2O$, $MnSO_4{\cdot}1H_2O$	[15–17]
$MgSO_4$–H_2O	$\gamma_{\pm}$-a_{water}-solubility	0–250	$MgSO_4{\cdot}7H_2O$, $MgSO_4{\cdot}6H_2O$, $MgSO_4{\cdot}1H_2O$	[17–19]
Na_2SO_4–H_2O	$\gamma_{\pm}$-a_{water}-solubility	0–240	$Na_2SO_4{\cdot}10H_2O$, Na_2SO_4	[17,18,20–23]
$ZnSO_4$–H_2O	$\gamma_{\pm}$-a_{water}-solubility	0–300	$ZnSO_4{\cdot}7H_2O$, $ZnSO_4{\cdot}6H_2O$, $ZnSO_4{\cdot}1H_2O$	[17,24,25]
$NiSO_4$–H_2O	$\gamma_{\pm}$-solubility	0–300	$NiSO_4{\cdot}7H_2O$, $NiSO_4{\cdot}6H_2O$, $NiSO_4{\cdot}1H_2O$	[17,24,26]
$CaSO_4$–H_2O	Solubility	0–300	$CaSO_4{\cdot}2H_2O$, $CaSO_4{\cdot}0.5H_2O$, $CaSO_4$	[17,27–36]
Ternary systems				
$CaSO_4$–H_2SO_4–H_2O	Solubility	25–300	$CaSO_4{\cdot}2H_2O$, $CaSO_4{\cdot}0.5H_2O$, $CaSO_4$	[32,33,37–39]
$CaSO_4$–$MgSO_4$–H_2O	Solubility	25–175	$CaSO_4{\cdot}2H_2O$, $CaSO_4{\cdot}0.5H_2O$, $CaSO_4$	[6,17,40–42]
$CaSO_4$–$ZnSO_4$–H_2O	Solubility	25–200	$CaSO_4{\cdot}2H_2O$, $CaSO_4{\cdot}0.5H_2O$, $CaSO_4$	[40,43]
$CaSO_4$–Na_2SO_4–H_2O	Solubility	25–300	$CaSO_4{\cdot}2H_2O$, $CaSO_4$	[17,29,36,44–48]
$CaSO_4$–$MnSO_4$–H_2O	Solubility	25–100	$CaSO_4{\cdot}2H_2O$	[49]
$CaSO_4$–$(NH_4)_2SO_4$–H_2O	Solubility	25–100	$CaSO_4{\cdot}2H_2O$, $CaSO_4$	[17]
$CaSO_4$–$NiSO_4$–H_2O	Solubility	25–90	$CaSO_4{\cdot}2H_2O$	[50]
$Fe_2(SO_4)_3$–H_2SO_4–H_2O	Solubility	25–140	$Fe_2(SO_4)_3{\cdot}9H_2O$, $Fe_2(SO_4)_3{\cdot}6H_2O$, $Fe_2(SO_4)_3$	[51–53]
$MnSO_4$–H_2SO_4–H_2O	Solubility	25–65	$MnSO_4{\cdot}1H_2O$	[17]
$ZnSO_4$–H_2SO_4–H_2O	Solubility	15–70	$ZnSO_4{\cdot}7H_2O$, $ZnSO_4{\cdot}6H_2O$, $ZnSO_4{\cdot}1H_2O$	[17]

Table 2
Multi-component systems studied for the chemical modelling validation of $CaSO_4$ in sulphate solutions

System	Data type	Temperature range (°C)	Solid phases	References
Multi-component systems				
$CaSO_4$–$ZnSO_4$–H_2SO_4 (0.1 M)–H_2O	Solubility	25–90	$CaSO_4·2H_2O$	[33]
$CaSO_4$–H_2SO_4–$ZnSO_4$ (1.5 M)–H_2O	Solubility	25–90	$CaSO_4·2H_2O$	[33]
$CaSO_4$–Na_2SO_4–H_2SO_4–H_2O	Solubility	45–80	$CaSO_4·2H_2O$	[54]
$CaSO_4$–$MgSO_4$–$ZnSO_4$ (1.15 M)–H_2SO_4 (0.1 M)–H_2O	Solubility	25–90	$CaSO_4·2H_2O$	[33]
$CaSO_4$–$MgSO_4$–$ZnSO_4$ (1.15 M)–H_2SO_4 (0.3 M)–H_2O	Solubility	25–90	$CaSO_4·2H_2O$	[33]
$CaSO_4$–$Fe_2(SO_4)_3$–$ZnSO_4$ (1.15 M)–H_2SO_4 (0.3 M)–H_2O	Solubility	25–90	$CaSO_4·2H_2O$	[33]
$CaSO_4$–Na_2SO_4–$ZnSO_4$ (2.5 M)–$MgSO_4$ (0.41 M)–$MnSO_4$ (0.18 M)–H_2SO_4 (pH 3.8)–H_2O	Solubility	25–90	$CaSO_4·2H_2O$	[33]
$CaSO_4$–H_2SO_4–$ZnSO_4$ (2.5 M)–$MgSO_4$ (0.41 M)–$MnSO_4$ (0.18 M)–H_2O	Solubility	25–90	$CaSO_4·2H_2O$	[33]
$CaSO_4$–$(NH_4)_2SO_4$–$ZnSO_4$ (2.5 M)–$MgSO_4$ (0.41 M)–$MnSO_4$ (0.18 M)–H_2SO_4 (pH 3.8)–H_2O	Solubility	25–90	$CaSO_4·2H_2O$	[33]

systems, and validation of the parameters was performed by predicting the chemistry of quaternary or multi-component systems that were not used in the regression stage. A list of the different systems studied in this work is given in Table 1.

Multi-component systems used for the validation of the estimated parameters of the new model are listed in Table 2. These systems were not used to determine the parameters of the model, and they are shown to be accurately predictable with the new model-obtained parameters.

Table 3 presents the absolute average relative deviation (AARD%) between experimental data and calculated results obtained from the model for the systems studied in this work.

3. Results and discussion

The obtained model parameters are presented in Appendix A. Also, the regressed values for the standard state Gibbs free energy, entropy and coefficients of the heat capacity of the different solids studied are shown in Appendix B. The following section will discuss the results for the estimation of the binary and ternary parameters as well as the prediction of the multi-component systems and model validation.

3.1. Binary systems (metal sulphate–H_2O)

The solubility of different metal sulphates (shown in Table 1) was verified to determine whether the default databank of the OLI system is capable of reproducing the available experimental data, or whether it was necessary to perform an estimation of the parameters through the OLI built-in regression feature.

3.1.1. $CaSO_4$–H_2O system

The solubility of $CaSO_4$ solid phases (dihydrate, hemihydrate and anhydrite) has been extensively measured (dihydrate: [27–33]; hemihydrate: [17,34,35]; anhydrite: [30,31,34,36]). Most of the measurements are in fairly good agreement with each other. These experimental solubility data were used to verify the OLI default databank.

Although the solubility of $CaSO_4$ dihydrate (gypsum) in H_2O from 0 to 110 °C (Fig. 1) can be calculated accurately with the OLI default database (version 7.0.41) using the MSE model, there are no data for hemihydrate ($CaSO_4·0.5H_2O_{(s)}$) in the OLI default database. Therefore, literature solubility data [17,34,35] were used to adjust the standard state Gibbs free energy, the entropy and the heat capacity of the solid as a function of temperature up to 200 °C. The regressed solubility curve is presented in Fig. 2.

Contrary to hemihydrate, experimental data on the solubility of anhydrite ($CaSO_{4(s)}$) in water are available and are shown in Fig. 3. The OLI default database can accurately reproduce all the experimental data over a wide temperature range from 0 to 300 °C.

3.1.2. Calcium sulphate–water phase diagram

Fig. 4 shows the solubility of the three phases of $CaSO_4$ on one graph. It can be seen that below ~40 °C, gypsum has the lowest solubility and is therefore the most thermodynamically stable phase. The transition point of gypsum to anhydrite lies at 40 ± 2 °C, and that of gypsum to hemihydrate lies at 99 ± 2 °C. In the region between these two temperatures, gypsum is metastable, although the degree of metastability in dilute

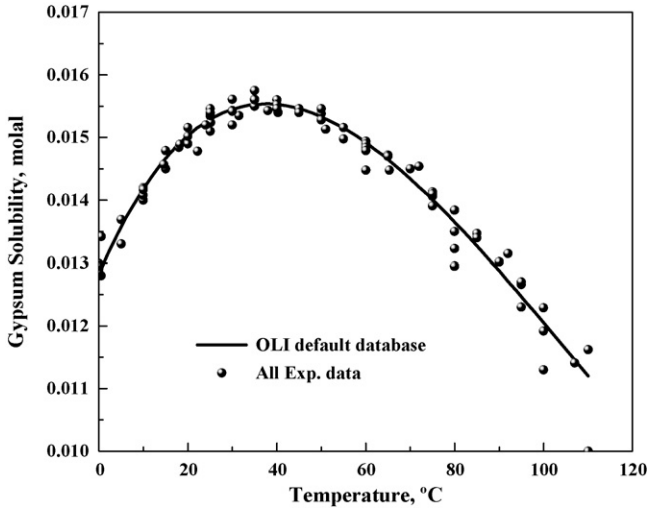

Fig. 1. Dihydrate solubility in H_2O vs. temperature. Experimental data are from [27–33]; the curve is determined from the OLI default database.

Table 3
Absolute average relative deviation (AARD%) between experimental data and calculated results from the model

System	Temperature range (°C)	AARD (%)[a]
$MnSO_4$–H_2O	0–180	2.6
$NiSO_4$–H_2O	0–300	4.7
$CaSO_4$–H_2O (only hemihydrate solubility)	0–200	4.9
$CaSO_4$–$(NH_4)_2SO_4$–H_2O	25–100	3.9
$Fe_2(SO_4)_3$–H_2SO_4–H_2O	25–140	4.4
$CaSO_4$–$MnSO_4$–H_2O	25–100	5.9
$CaSO_4$–$MgSO_4$–H_2O	25–175	5.7
$CaSO_4$–Na_2SO_4–H_2O	25–300	4.6
$MnSO_4$–H_2SO_4–H_2O	25–65	6.1
$CaSO_4$–H_2SO_4–H_2O	25–300	7.8
$CaSO_4$–$ZnSO_4$–H_2O	25–200	5.2
$CaSO_4$–$NiSO_4$–H_2O	25–90	3.5
$CaSO_4$–$ZnSO_4$–H_2SO_4 (0.1 M)–H_2O	25–90	5.8
$CaSO_4$–H_2SO_4–$ZnSO_4$ (1.5 M)–H_2O	25–90	6.3
$CaSO_4$–Na_2SO_4–H_2SO_4–H_2O	45–80	7.5
$CaSO_4$–$MgSO_4$–$ZnSO_4$ (1.15 M)–H_2SO_4 (0.1 M)–H_2O	25–90	3.5
$CaSO_4$–$MgSO_4$–$ZnSO_4$ (1.15 M)–H_2SO_4 (0.3 M)–H_2O	25–90	8.5
$CaSO_4$–$Fe_2(SO_4)_3$–$ZnSO_4$ (1.15 M)–H_2SO_4 (0.3 M)–H_2O	25–90	6.5
$CaSO_4$–Na_2SO_4—$ZnSO_4$ (2.5 M)–$MgSO_4$ (0.41 M)–$MnSO_4$ (0.18 M)–H_2SO_4 (pH 3.8)–H_2O	25–90	5.4
$CaSO_4$–H_2SO_4–$ZnSO_4$ (2.5 M)–$MgSO_4$ (0.41 M)–$MnSO_4$ (0.18 M)–H_2O	25–90	5.2
$CaSO_4$–$(NH_4)_2SO_4$–$ZnSO_4$ (2.5 M)–$MgSO_4$ (0.41 M)–$MnSO_4$ (0.18 M)–H_2SO_4 (pH 3.8)–H_2O	25–90	4.5

[a] $\text{AARD}\,(\%) = (100/\text{NP})\sum_{i}^{\text{NP}}(|\text{Exp. data} - \text{calculated value}|)/\text{Exp. data}$, NP: no. of experimental points.

aqueous solutions is significant. Thus, gypsum–water slurries can be heated to 100 °C without the transformation of gypsum to anhydrite or hemihydrate, and identical solubilities are measured on heating and cooling. In contrast, gypsum transforms rapidly to anhydrite in concentrated acid–salt solutions at temperatures above about 60 °C [33], and in such concentrated solutions, lower $CaSO_4$ concentrations are measured on cooling than on heating.

In regard to the transition point of hemihydrate to anhydrite, no definitive experimental evidence is available. The ease with which anhydrite takes up water vapour to change to hemihydrate has been interpreted to indicate that the dissociation pressure is very low, and that the transition point probably lies at a relatively high temperature [30]. Attempts to determine this dissociation pressure curve by direct measurements have so far been unsuccessful, because of the instability of the hemihydrate phase.

3.1.3. $MnSO_4$–H_2O system

There are no relevant data for $MnSO_4$ in the OLI default database. Therefore, experimental data on the solubility of $MnSO_4$ in H_2O [17], the mean activity coefficient ($\gamma_\pm$) [15], the activity of water (a_{water}) [15] and heat capacity (C_p) [16] were used to regress model parameters including the

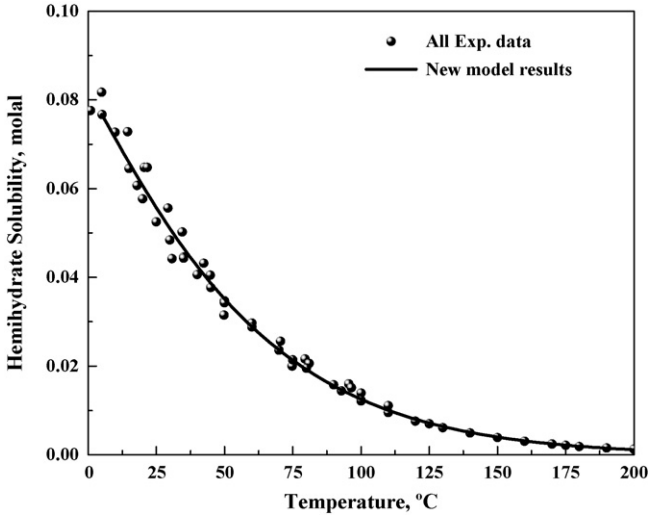

Fig. 2. Hemihydrate solubility in H_2O vs. temperature. Experimental data are from [17,34,35]; the curve is the regressed model results.

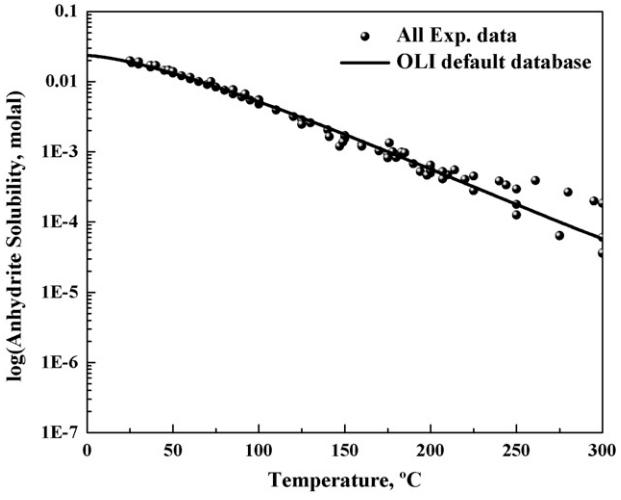

Fig. 3. Anhydrite solubility in H_2O vs. temperature. Experimental data are from [30,31,34,36]; the curve is the OLI default database results.

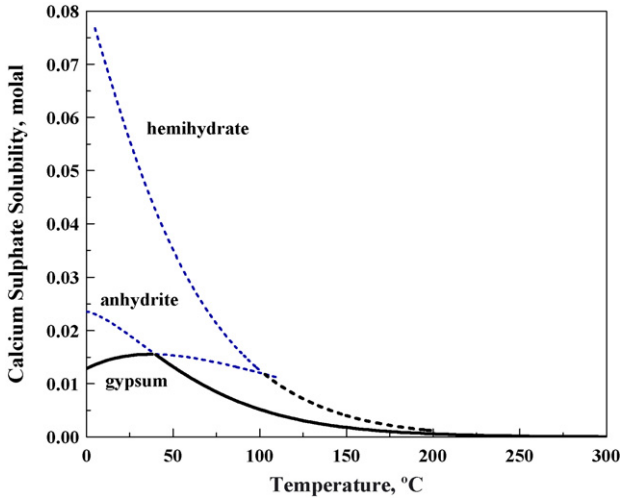

Fig. 4. The phase transition diagram of $CaSO_4$ in H_2O. The solid and dashed curves show the stable and metastable phases, respectively, at each temperature.

standard state Gibbs free energy, the entropy and the heat capacity of the solids; i.e., $MnSO_4{\cdot}7H_2O$, $MnSO_4{\cdot}5H_2O$ and $MnSO_4.1H_2O$ as a function of temperature. In addition, MSE ionic interaction parameters between Mn^{2+} and SO_4^{2-} ions were regressed. The solubility curve of this system is shown in Fig. 5.

3.1.4. $NiSO_4$–H_2O system

Experimental data on the mean activity coefficient, the activity of water and the solubility of aqueous $NiSO_4$ [17,24,26] were used to fit the MSE middle range interaction parameters between Ni^{2+} and SO_4^{2-} ions, as well as the standard state Gibbs free energy, and the entropy of solid $NiSO_4{\cdot}7H_2O$, $NiSO_4.6H_2O$, and $NiSO_4{\cdot}1H_2O$ as a function of temperature. Fig. 6 shows the solubility of $NiSO_4$ in H_2O up to 250 °C.

No additional fitting was carried out on the $MgSO_4$, $ZnSO_4$ and Na_2SO_4 aqueous metal sulphate system, because the OLI default database was found to predict these systems accurately.

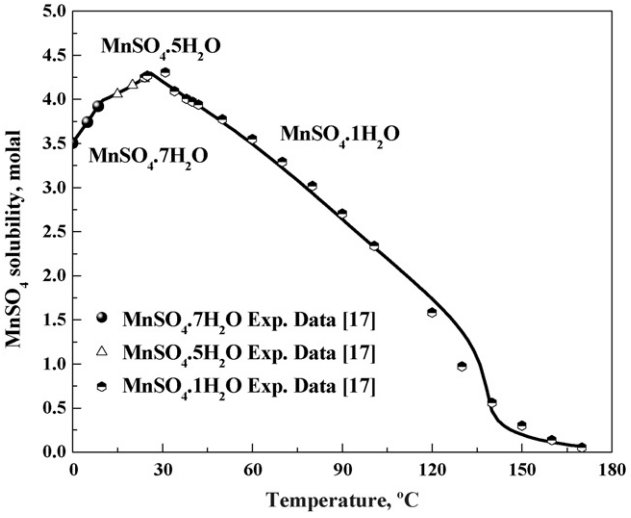

Fig. 5. The solubility of $MnSO_4$ in H_2O; the curve shows the model results.

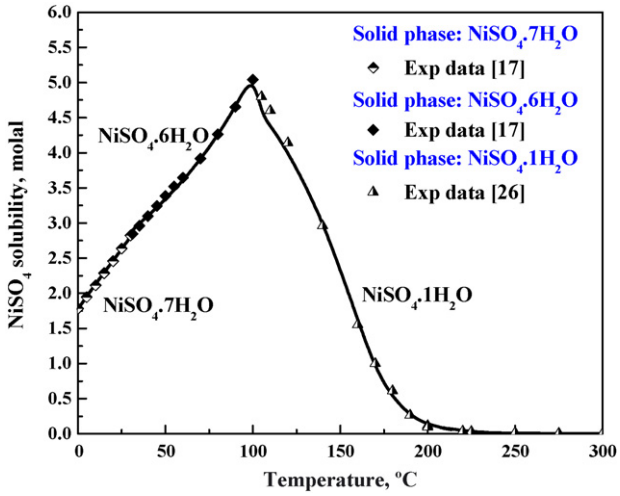

Fig. 6. The solubility of $NiSO_4$ in H_2O; the curve shows the model results.

3.1.5. $Fe_2(SO_4)_3$–H_2O system

No reliable data are available on the solubility of $Fe_2(SO_4)_3$ in water, the mean activity coefficient of $Fe_2(SO_4)_3$ solutions and the activity of water.

The solubility in this system is difficult to study mainly because of the pronounced tendency of $Fe_2(SO_4)_3$ to hydrolyse in aqueous solutions and form a variety of precipitates. The solutions formed are a yellow-brown colour, because of the presence of iron(III)–hydroxyl ions (hydrated Fe^{3+} ions are nearly colourless) [55].

3.2. Ternary systems

In this section, different ternary systems are investigated. In most of the case studies, the interactions between the different dominant species are significant and need to be taken into account. Therefore, extra MSE ion interaction parameters were regressed for better performance of the model. Most of the work described below focuses on the impact of foreign electrolytes on the $CaSO_4$ solubility behaviour.

3.2.1. $CaSO_4$–H_2SO_4–H_2O system

The solubility of $CaSO_4$ hydrates in H_2SO_4 solutions has been measured by Ling and Demopoulos [37], Dutrizac [33], Zdanovskii et al. [38,39] and Marshall et al. [32]. The OLI default database does not predict the solubility behaviour in this system very accurately. Consequently, experimental data for gypsum, hemihydrate and anhydrite were used to regress the MSE middle range interaction parameters between Ca^{2+} and HSO_4^- over a wide temperature range, from 25 to 300 °C. As shown in Figs. 7–9, the model fits the data closely for all temperatures and for all three solids, in spite of the often complex solubility–temperature relationships. Fig. 10 shows the three-dimensional phase transition diagram of this system.

At low temperatures (25–60 °C), the addition of H_2SO_4 increases the solubility of $CaSO_4{\cdot}2H_2O$ moderately, whereas at very high concentrations of acid, the solubility is decreased. However, at higher temperatures, the solubility increases

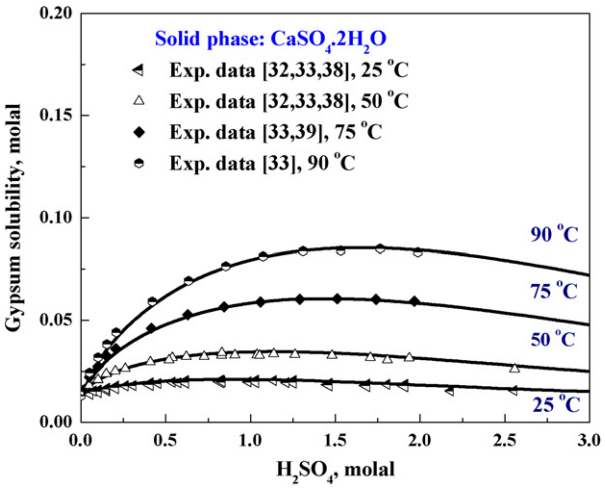

Fig. 7. Gypsum solubility in H_2SO_4 solutions at different temperatures; experimental data are from [32,33,38,39], and the curves are the fitted model.

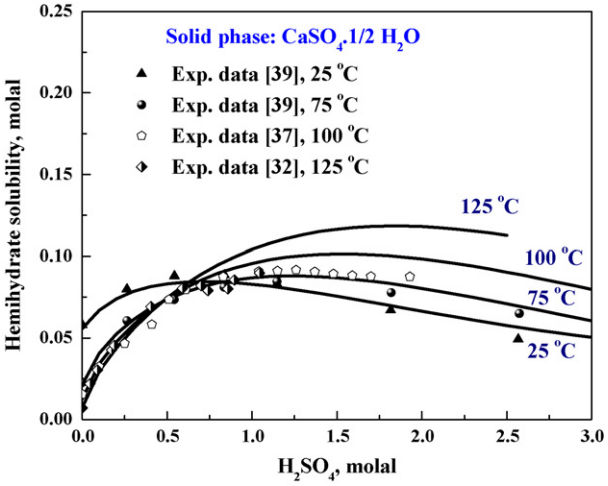

Fig. 8. Hemihydrate solubility in H_2SO_4 solutions at different temperatures; experimental data are from [32,37,39], and the curves are the fitted model.

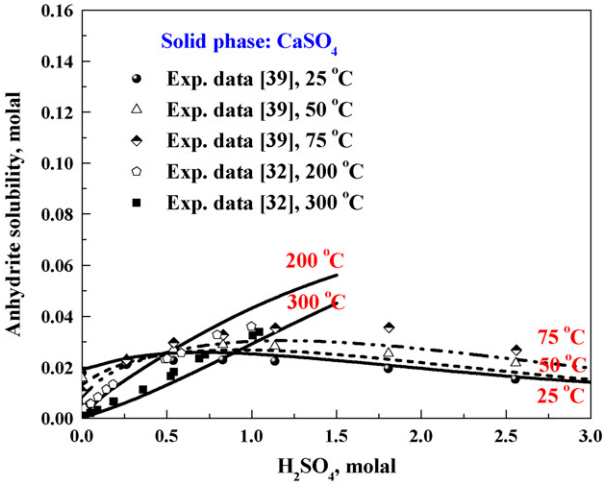

Fig. 9. Anhydrite solubility in H_2SO_4 solutions at different temperatures; experimental data are from [32,39], and the curves are the fitted model.

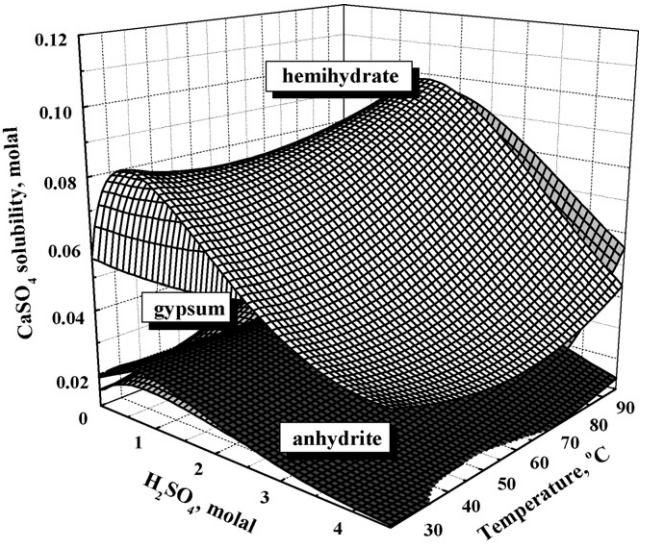

Fig. 10. The phase transition diagram of $CaSO_4$ in H_2SO_4 solutions.

strongly with increasing acid concentration. The behaviour in dilute to moderately high acid concentrations is due to the decrease of the second dissociation constant of H_2SO_4 with increasing temperature. Thus, the addition of H_2SO_4 to saturated $CaSO_4$–H_2O solutions reduces the SO_4^{2-} concentration and allows an increase in the solubility of $CaSO_4$ to satisfy the solubility product. This increase is also due to the increase in the ionic strength caused by the addition of the acid [32].

The solubility isotherms obtained at 25, 50, 75 and 95 °C are presented in Figs. 11–14. Despite the often complex solubility relationships, the model calculates the solubilities with a good degree of accuracy. There are two possible phase transitions among the different calcium sulphate solid phases, gypsum to anhydrite and gypsum to hemihydrate, as follows:

$$CaSO_4{\cdot}2H_2O \leftrightarrow CaSO_4{+}2H_2O \quad (14)$$

$$CaSO_4{\cdot}2H_2O \leftrightarrow CaSO_4{\cdot}0.5H_2O + 1.5H_2O \quad (15)$$

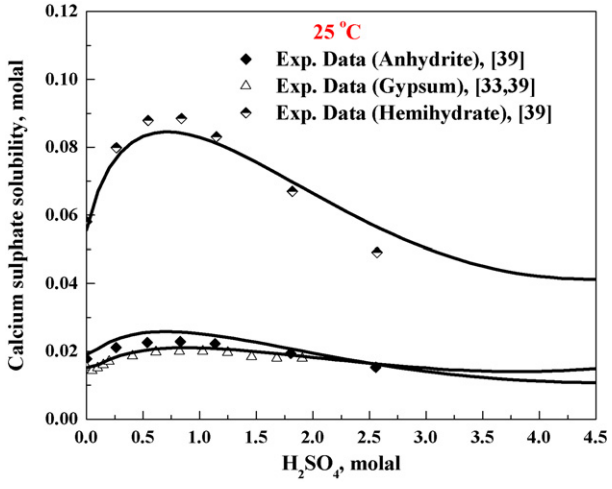

Fig. 11. The solubility of $CaSO_4$ hydrates in H_2SO_4 solutions at 25 °C; experimental data are from [33,39], and the curves are the fitted model.

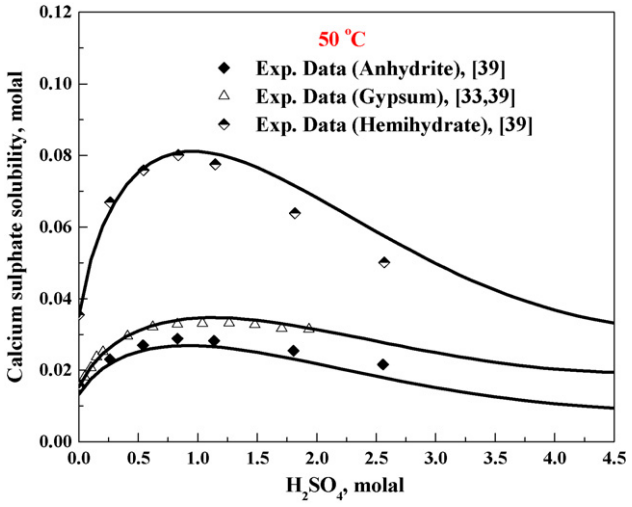

Fig. 12. The solubility of $CaSO_4$ hydrates in H_2SO_4 solutions at 50 °C; experimental data are from [33,39], and the curves are the fitted model.

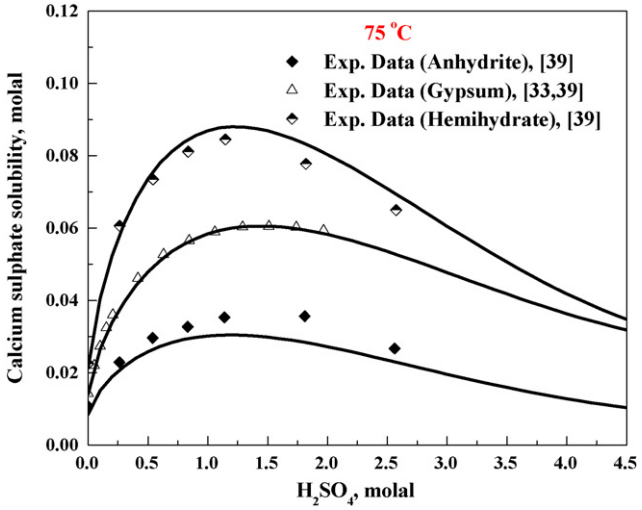

Fig. 13. The solubility of $CaSO_4$ hydrates in H_2SO_4 solutions at 75 °C; experimental data are from [33,39], and the curves are the fitted model.

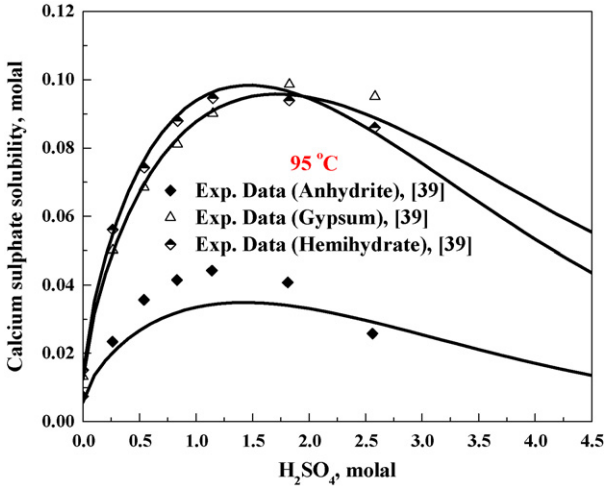

Fig. 14. The solubility of $CaSO_4$ hydrates in H_2SO_4 solutions at 95 °C; experimental data are from [33,39], and the curves are the fitted model.

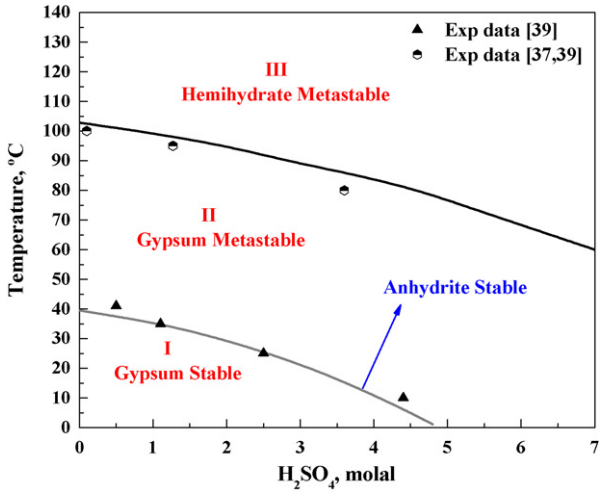

Fig. 15. The $CaSO_4$ phase transition diagram in ternary system of $CaSO_4$–H_2SO_4–H_2O system. Region I: gypsum stable, Region II: anhydrite stable, gypsum metastable, Region III: anhydrite stable, hemihydrate metastable. Experimental data are from [37,39].

The phase transition between gypsum-anhydrite and gypsum-hemihydrate was determined on the basis of phase solubilities. At the transition point, where there is equilibrium between two phases, the solubility of both phases is equal. Fig. 15 shows the phase transition diagram that was obtained on the basis of the solubility curves calculated from the new model. In order to validate this diagram, some available experimental points which were measured by Zdanovskii et al. [39] up to 95 °C and Ling and Demopoulos [37] at 100 °C were used. It is clear from the figure that the agreement between the experimental points and new model results is very good. Also, it can be seen that at 25 °C gypsum is the stable phase up to 4.7m of acid concentration. The gypsum-anhydrite and gypsum-hemihydrate phase transitions take place around 40 and 100 °C, respectively.

3.2.2. *$CaSO_4$–$MgSO_4$–H_2O system*

The solubility of calcium sulphate dihydrate in magnesium sulphate solutions at different temperatures was measured by Arsalan and Dutt [6], Umetsu et al. [40], Tanji [41] and Novikova [42]. Also, Linke and Seidell [17] collected a large number of experimental solubility data of electrolyte solutions which were used in this work. For this system, new MSE middle range interaction parameters between Ca^{2+} and Mg^{2+} as well as $CaSO_{4(aq)}{}^0$ and Mg^{2+} species were fitted. In this system, Ca^{2+} is the dominant species at lower concentrations of $MgSO_4$, whereas at higher concentrations, the neutral calcium sulphate ion pair, $CaSO_{4(aq)}{}^0$, becomes dominant.

Umetsu et al. [40] also measured the solubility of calcium sulphate hydrates at temperatures between 100 and 175 °C. These data were used to widen the applicability range of the MSE middle range parameters between Ca species and Mg^{2+} ions. The results obtained are shown in Figs. 16 and 17. The model accurately reflects the experimental data.

Umetsu et al. [40] observed that gypsum was the stable solid phase in their experiments up to 75 °C. It then transformed to hemihydrate at ~100–110 °C, and to anhydrite above 150 °C.

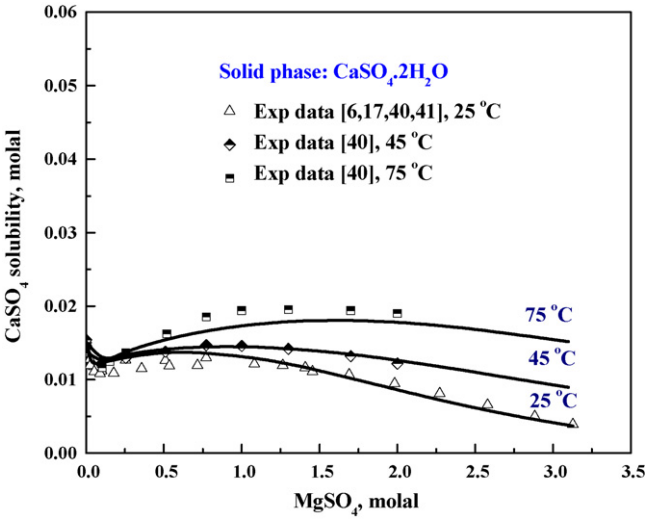

Fig. 16. $CaSO_4$ solubility in $MgSO_4$ solutions at temperatures below 100 °C; experimental data are from [6,17,40,41], and the curves are the fitted model.

However, the present model shows that their experimental data, even above 150 °C, closely matches the solubility of hemihydrate instead of that of anhydrite.

3.2.3. $CaSO_4$–$ZnSO_4$–H_2O system

The $CaSO_4$–$ZnSO_4$–H_2O system was studied by Umetsu et al. [40] and Zatonskaya et al. [43] over a wide temperature range from 25 to 200 °C. Their experimental solubility data were used to regress the MSE middle range interaction parameters between the dominant species in the solution; that is, Zn^{2+} and Ca^{2+} at lower $ZnSO_4$ concentrations, and Zn^{2+} and $CaSO_{4(aq)}{}^0$ at higher concentrations of $ZnSO_4$.

As mentioned earlier, the data reported for the solubility of anhydrite above 150 °C by Umetsu et al. [40] are actually related to those of hemihydrate in the present study. Nevertheless, it is clear from Figs. 18 and 19 that the model is capable of accurately estimating the solubility data for this system.

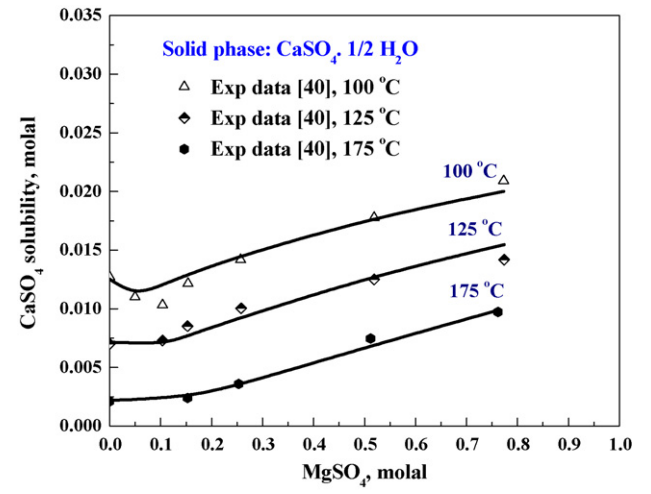

Fig. 17. $CaSO_4$ solubility in $MgSO_4$ solutions at temperatures above 100 °C; experimental data are from [40], and the curves are the fitted model.

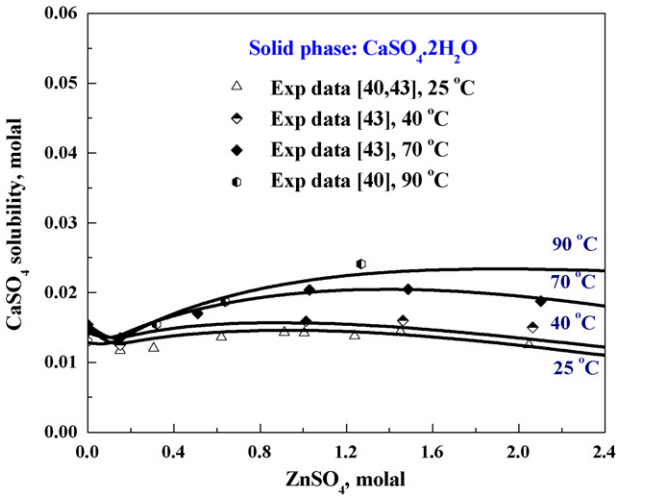

Fig. 18. $CaSO_4$ solubility in $ZnSO_4$ solutions at temperatures below 100 °C; experimental data are from [40,43], and the curves are the regressed model.

3.2.4. $CaSO_4$–Na_2SO_4–H_2O system

The solubility of $CaSO_4$ hydrates in aqueous solutions of Na_2SO_4 was studied by Supatashvili et al. [44], Block and Waters [45], Templeton et al. [46], Denman [47], Hill and Wills [29], Silcock [48], Straub [36], and is also cited by Linke and Seidell [17] in their solubility data collection. The chemical behaviour of this system becomes complicated because of the formation of double salts of $CaSO_4$ and Na_2SO_4 such as $CaSO_4{\cdot}Na_2SO_4$ or $CaSO_4{\cdot}2Na_2SO_4{\cdot}2H_2O$ at high Na_2SO_4 concentrations. However, although these salts are thermodynamically more stable than gypsum, their formation kinetics were found to be extremely slow. Weeks are required to form the double salts in the absence of seeding [29]. Thus, gypsum was considered as the dominant phase in this system.

Figs. 20 and 21 present the solubility of $CaSO_4$ as a function of the concentration of Na_2SO_4 for both the dihydrate (gypsum) and anhydrite, respectively. Additional fitting was done on this system to attain Ca^{2+}–Na^+ MSE parameters. As

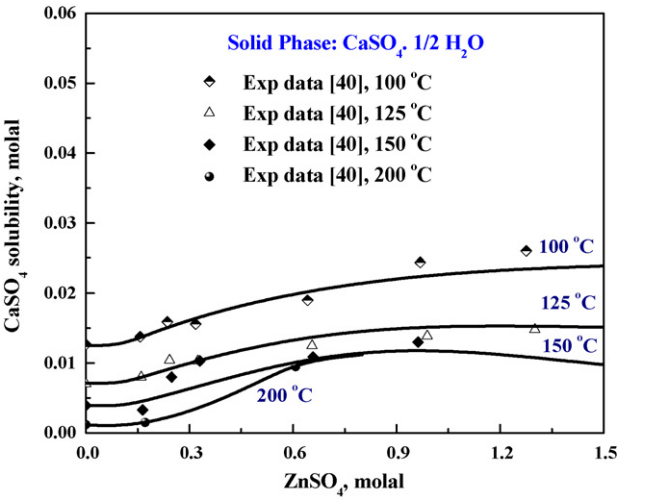

Fig. 19. $CaSO_4$ solubility in $ZnSO_4$ solutions at temperatures above 100 °C; experimental data are from [40], and the curves are the regressed model.

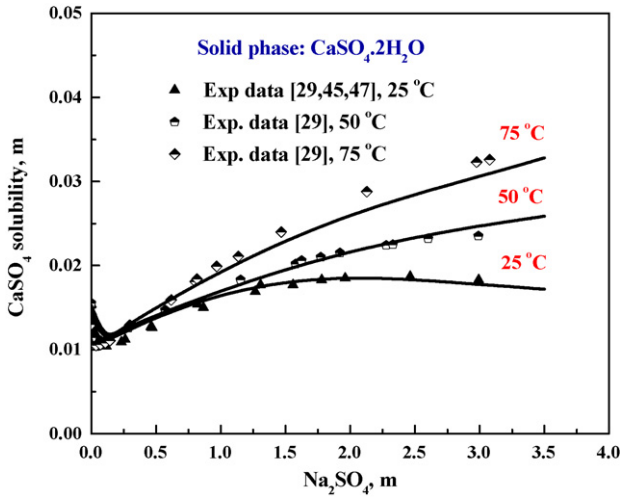

Fig. 20. $CaSO_4$ solubility in Na_2SO_4 solutions at temperatures below 100 °C; experimental data are from [29,45,47], and the curves are the fitted model. Dihydrate (gypsum) is the saturating solid phase.

is clear from the figures, the obtained fits are in excellent agreement with the experimental results, even where the solubility data show a complex relationship with increasing Na_2SO_4 concentration.

3.2.5. $CaSO_4$–$MnSO_4$–H_2O system

Zhelnin et al. [49] measured the solubility of $CaSO_4$ in the $CaSO_4$–$MnSO_4$–H_2O system from room temperature to 100 °C, and their observations show that in this temperature range, even up to 3.5m $MnSO_4$, gypsum is the only solid in equilibrium with the solution. The experimental data were used to fit Ca^{2+}–Mn^{2+} and also $CaSO_{4(aq)}{}^0$–Mn^{2+} MSE interaction parameters, because in higher concentrations of $MnSO_4$, $CaSO_{4(aq)}{}^0$ is more abundant than the Ca^{2+} species. The fitted results for this system are shown in Fig. 22, and the calculated solubilities are very consistent with the experimental data.

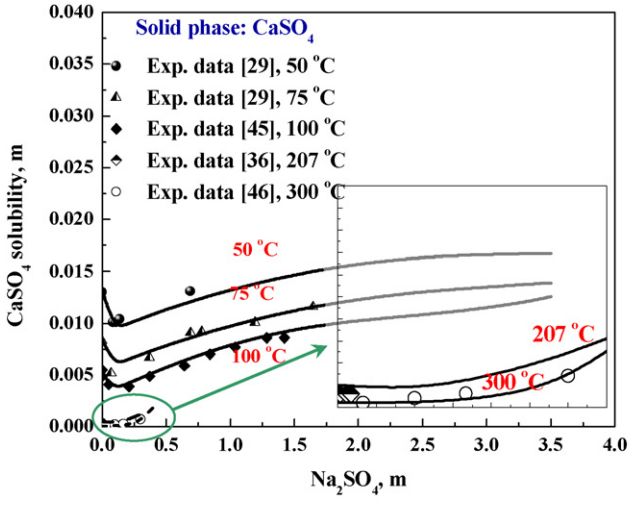

Fig. 21. $CaSO_4$ solubility in Na_2SO_4 solutions at temperatures above 100 °C; experimental data are from [29,36,45,46], and the curves are the fitted model. Anhydrite is the saturating solid phase.

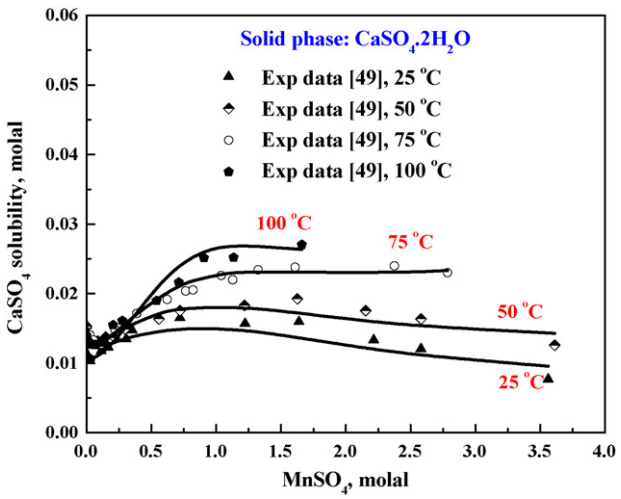

Fig. 22. $CaSO_4$ solubility in $MnSO_4$ solutions; experimental data are from [49], and the curves are the fitted model.

3.2.6. $CaSO_4$–$(NH_4)_2SO_4$–H_2O system

The experimental data for this system were selected from the Linke and Seidell [17] solubility data collection. For this system, data are available for gypsum over a temperature range of 25–100 °C, and for anhydrite from 75 to 100 °C. Additional fitting was needed for Ca^{2+}–$NH_4{}^+$ and $CaSO_{4(aq)}{}^0$–$NH_4{}^+$ MSE parameters in order to achieve an accurate performance of the model. Fig. 23 shows the regressed results from the model which are in good agreement with the experimental data.

3.2.7. $CaSO_4$–$NiSO_4$–H_2O system

Campbell and Yanick [50] studied the solubility of $CaSO_4$ in aqueous solutions of $NiSO_4$ over the temperature range from 45 to 90 °C. Because the OLI default database did not accurately reflect these data, MSE parameters were fitted between Ca^{2+} and Ni^{2+} ions in the solution using the experimental solubility data. The fitted model results are shown in Fig. 24. As can be seen, model prediction is very good compared with the experimental data.

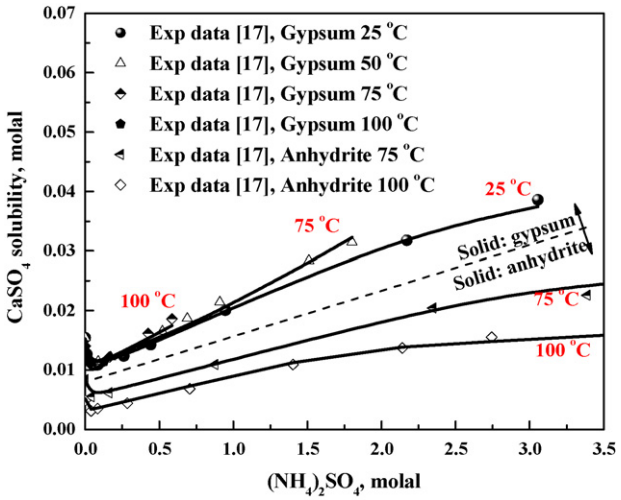

Fig. 23. $CaSO_4$ solubility in $(NH_4)_2SO_4$ solutions; experimental data are from [17], and the curves are the fitted model.

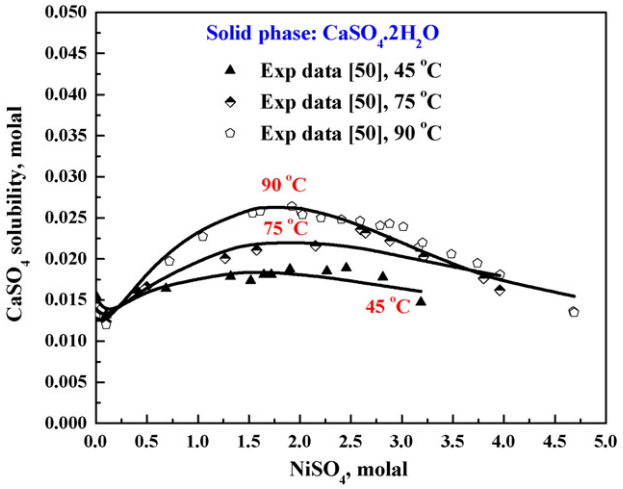

Fig. 24. $CaSO_4$ solubility in $NiSO_4$ solutions; experimental data are from [50], and the curves are the regressed model results.

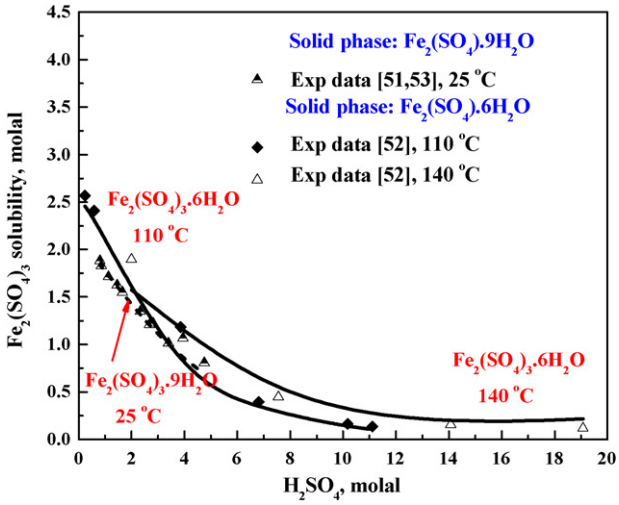

Fig. 25. $Fe_2(SO_4)_3$ solubility in H_2SO_4 solutions; experimental data are from [51–53], and the curves are the regressed model results.

As the $NiSO_4$ concentration increases from pure water, the solubility of $CaSO_4$ initially drops because of the common ion effect (SO_4^{2-} is added) which shifts the reaction of $CaSO_4{\cdot}nH_2O_{(s)} = Ca^{2+} + SO_4^{2-} + nH_2O$ to the left. However, for $NiSO_4$ concentrations above about 0.25m, this effect is nullified by the increasing ion interaction or association between $Ca^{2+}$and SO_4^{2-}. Also, the solubility of $CaSO_4$, which decreases with increasing temperatures above about 40 °C in water, becomes positively related to temperature at high sulphate concentrations. The same behaviour was also observed for the solubility of $CaSO_4$ in other metal sulphate systems such as those containing $MgSO_4$, $ZnSO_4$, etc.

3.2.8. $Fe_2(SO_4)_3$–H_2SO_4–H_2O system

The solubility of $Fe_2(SO_4)_3$ in aqueous sulphuric acid solutions was studied by Baskerville and Cameron [51], Posnjak and Merwin [52] and Wirth and Bakke [53]. Different solids exist in the system depending on the solution conditions such as pH and temperature. At temperatures below 100 °C, the solid phase is $Fe_2(SO_4)_3{\cdot}9H_2O$, whereas at higher temperatures, it transforms to $Fe_2(SO_4)_3{\cdot}6H_2O$, and even to $Fe_2(SO_4)_3$ around 200 °C. Additional fittings were performed for the $Fe^{3+} - HSO_4^-$ MSE middle range parameters to improve the prediction of the chemistry for the system. The results obtained from the fitting compared with the experimental data over a temperature range of 25–200 °C are shown in Fig. 25. As is clear, the model results are very consistent with the experimental data.

3.2.9. $MnSO_4$–H_2SO_4–H_2O system

The experimental data for this system were selected from the Linke and Seidell [17] solubility data collection. Regression was performed on the MSE parameters between the $Mn^{2+} - HSO_4^-$ and $MnSO_{4(aq)}{}^0 - HSO_4^-$ species to allow an acceptable model prediction. The fitted results corresponding to the experimental data are shown in Fig. 26, and as can be seen, the results are generally consistent with the experimental results.

3.3. Quaternary systems

So far, it has been shown that the MSE activity model works well for fitting the solubility trends for $CaSO_4$ hydrates in sulphate systems. However, validation of the model can be achieved only by predicting the solubility in multi-component systems in which no fitting was carried out. Accordingly, the solubility of $CaSO_4$ was calculated in multi-component aqueous systems including H_2SO_4, $ZnSO_4$, $MgSO_4$, $MnSO_4$, Na_2SO_4, etc. As will be seen further in this section, the model is capable of accurately predicting the chemistry in all the multi-component systems studied.

3.3.1. $CaSO_4$–$ZnSO_4$–H_2SO_4 (0.1 M)–H_2O system

Dutrizac [33] has studied the effect of $ZnSO_4$ concentration on the solubility of calcium sulphate in solutions containing 0.1 M H_2SO_4 as a function of temperature. The solubility of calcium sulphate decreases steadily as the $ZnSO_4$ concentra-

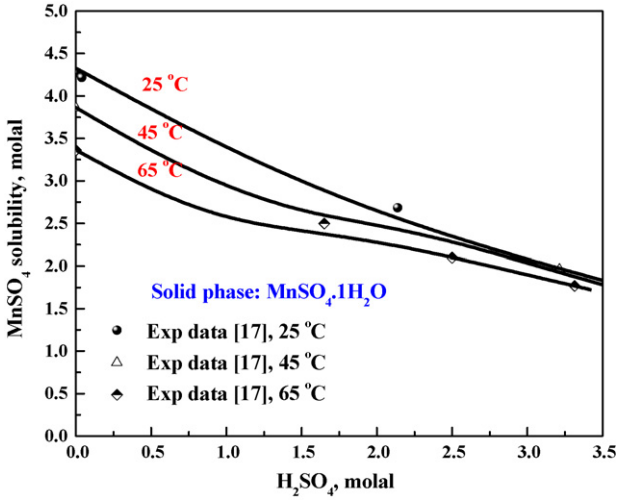

Fig. 26. $MnSO_4$ solubility in aqueous H_2SO_4 solutions; experimental data are from [17], and the curves are the regressed model results.

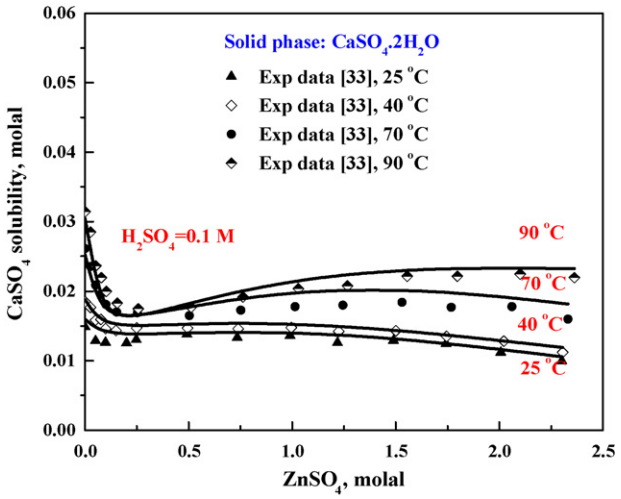

Fig. 27. $CaSO_4$ solubility in $CaSO_4$–$ZnSO_4$–H_2SO_4 (0.1 M)–H_2O solutions; the curves are the predicted values.

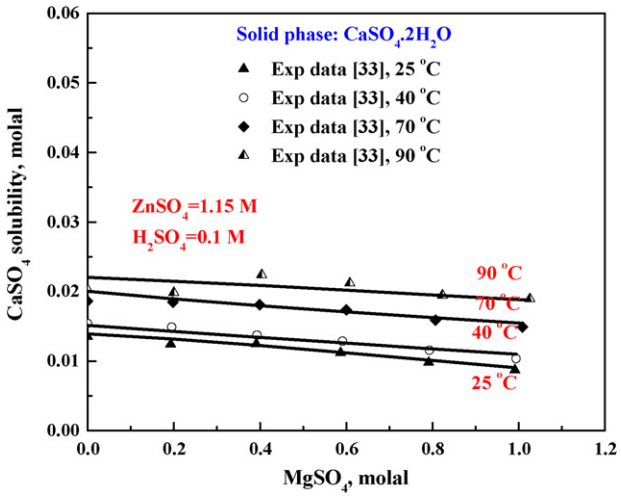

Fig. 29. $CaSO_4$ solubility in $CaSO_4$–$MgSO_4$–$ZnSO_4$ (1.15 M)–H_2SO_4 (0.1 M)–H_2O solutions; the curves are the predicted solubilities.

tion increases from 0.0 to 0.5 M $ZnSO_4$ because of the common ion effect. The experimental data were obtained on heating to 95 °C and on subsequent cooling. In this system, because the acid concentration used is relatively low, the dehydration of gypsum to anhydrite does not occur at temperatures below 95 °C. Fig. 27 shows the experimentally obtained $CaSO_4$ solubility versus $ZnSO_4$ concentration in 0.1 M H_2SO_4 media at different temperatures along with the model predictions. The predictions are in excellent agreement with the experimental results. Increasing $ZnSO_4$ concentration decreases the solubility of calcium sulphate at low temperatures because of bisulphate ion formation and the resulting decrease of the concentration of free SO_4^{2-} ions.

3.3.2. *$CaSO_4$–H_2SO_4–$ZnSO_4$ (1.5 M)–H_2O system*

The solubility of $CaSO_4$, as a function of acid concentration, was also measured by Dutrizac [33] in solutions containing 1.5 M $ZnSO_4$. Fig. 28 represents the experimental data and the predicted results from the model. As can be seen, the model prediction is in close agreement with the experimental data. The figure also shows that acid concentration has a relatively minor effect on the solubility of $CaSO_4$ when the solution contains 1.5 M of $ZnSO_4$. This effect is due to the free sulphate ions released from the dissociation of $ZnSO_4$.

3.3.3. *$CaSO_4$–$MgSO_4$–H_2SO_4 (0.1/0.3 M)–$ZnSO_4$ (1.15 M)–H_2O system*

Zinc processing solutions typically contain modest concentrations of $MgSO_4$ and of $MnSO_4$ [33]. The effect of $MgSO_4$ on the solubility of $CaSO_4$ was studied because its impact on $CaSO_4$ chemistry was unknown. For this purpose, the solubility of $CaSO_4$ in a system containing $MgSO_4$, $ZnSO_4$ and H_2SO_4 was modelled using the new database. As shown in Figs. 29 and 30, the model is able to predict these systems very closely compared with the experimental data. Also, it is obvious that in these solutions increasing $MgSO_4$

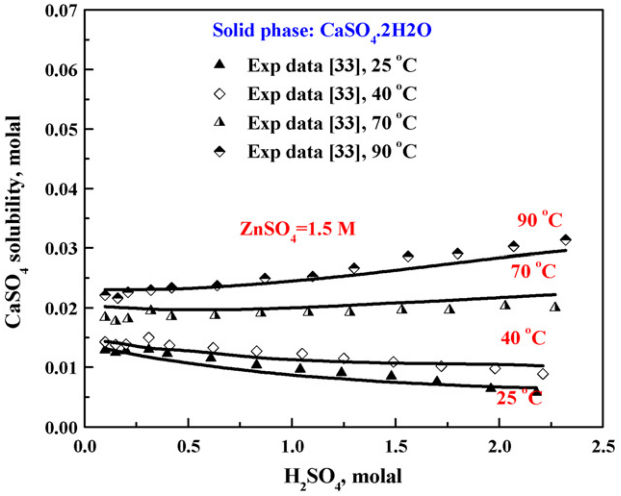

Fig. 28. $CaSO_4$ solubility in $CaSO_4$–H_2SO_4–$ZnSO_4$ (1.5 M)–H_2O solutions; the curves are the predicted values.

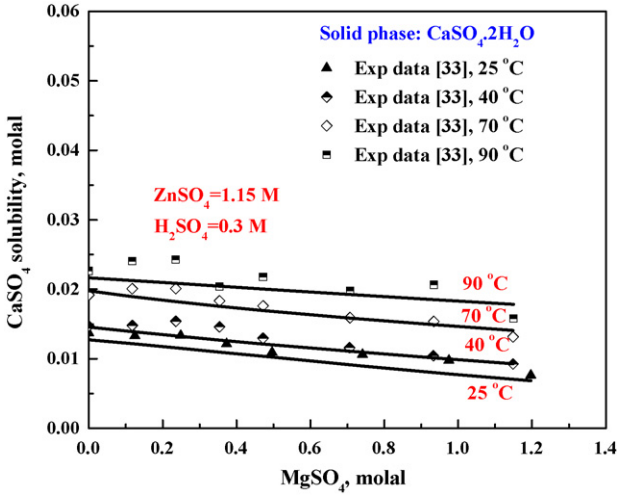

Fig. 30. $CaSO_4$ solubility in $CaSO_4$–$MgSO_4$–$ZnSO_4$ (1.15 M)–H_2SO_4 (0.3 M)–H_2O solutions; the curves are the predicted values.

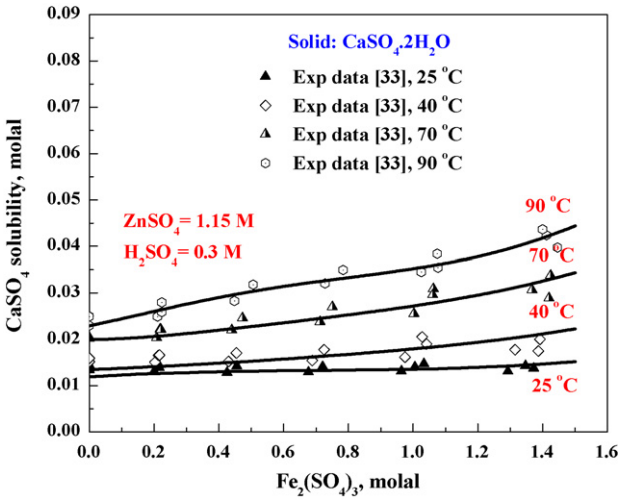

Fig. 31. $CaSO_4$ solubility in $CaSO_4$–$Fe_2(SO_4)_3$–H_2SO_4 (0.3 M)–$ZnSO_4$ (1.15 M)–H_2O solutions; curves are the fitted model predictions.

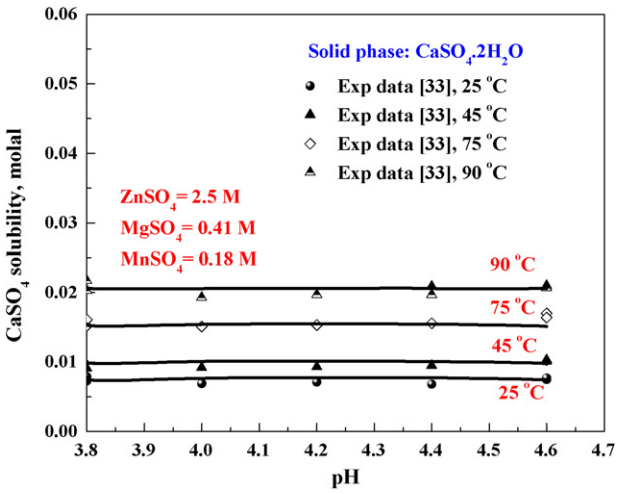

Fig. 32. $CaSO_4$ solubility in $CaSO_4$–H_2SO_4–$ZnSO_4$ (2.5 M)–$MgSO_4$ (0.41 M)–$MnSO_4$ (0.18 M)–H_2O solutions vs. pH; the curves are the predicted values.

concentrations have a negative impact on the solubility of $CaSO_4$.

3.3.4. $CaSO_4$–$Fe_2(SO_4)_3$–H_2SO_4 (0.3 M)–$ZnSO_4$ (1.15 M)–H_2O system

In the dominant roast–leach–electrolysis zinc process, iron present in the concentrate feed is oxidized to the ferric state in the roaster and is subsequently solubilized as ferric sulphate in the hot acid leaching sections of the process. Accordingly, the influence of dissolved ferric sulphate on the solubility of $CaSO_4$ is of some commercial importance.

Generally, the presence of ferric sulphate in the solution has only a modest effect on the solubility of $CaSO_4$. At higher temperatures, increasing $Fe_2(SO_4)_3$ concentrations cause a slight increase in the solubility of calcium sulphate.

There were no literature data available for the $CaSO_4$–$Fe_2(SO_4)_3$–H_2O system. Consequently, the experimental solubility data of $CaSO_4$ in aqueous solutions of $Fe_2(SO_4)_3$–H_2SO_4–$ZnSO_4$ measured by Dutrizac [33] were used to regress the MSE parameters of Fe^{3+}–Ca^{2+} and $Fe^{3+} - CaSO_{4(aq)}{}^0$ in order to allow a precise estimation of the chemistry of this system. The fitted results obtained for the solubility of $CaSO_4$ versus $Fe_2(SO_4)_3$ concentration are shown in Fig. 31 along with the experimental data. The model predictions accurately reflect the experimental data.

3.3.5. $CaSO_4$–H_2SO_4–$ZnSO_4$ (2.5 M)–$MgSO_4$ (0.41 M)–$MnSO_4$ (0.18 M)–H_2O system

To ascertain the effect of pH on the solubility of calcium sulphate under weakly acidic condition, a series of solubility measurements was carried out by Dutrizac [33] at various temperatures in solutions containing 2.5 mol/L $ZnSO_4$ as well as 0.41 mol/L $MgSO_4$ and 0.18 mol/L $MnSO_4$. The pH was varied from 3.6 to 4.6. The experimental solubility data for this system are shown in Fig. 32 along with the model predictions for the system. As can be seen, the agreement is very good. Also, it is clear that the $CaSO_4$ solubility does not change significantly with changing pH in a weakly acidic solution.

3.3.6. $CaSO_4$–$(NH_4)_2SO_4$–$ZnSO_4$(2.5 M)–$MgSO_4$ (0.41 M)–$MnSO_4$(0.18 M)–H_2SO_4 (pH 3.8)-H_2O system

High concentrations of $Fe_2(SO_4)_3$ are commonly generated in the hot acid leaching circuits of hydrometallurgical zinc operations [33]. At some point in the process, the dissolved iron must be eliminated, and the removal is most commonly carried out by the precipitation of jarosite-type compounds ($MFe_3(SO_4)_2(OH)_6$, where M is K, Na, NH_4, etc.). To form the jarosite precipitate, Na^+ or $NH_4{}^+$ ions are added to the solution, and inevitably, a circulating load of Na_2SO_4 or $(NH_4)_2SO_4$ results. The experimental measurements to investigate the effect of the concentration of Na_2SO_4 or $(NH_4)_2SO_4$ on the solubility of $CaSO_4$ were performed by Dutrizac [33]. As indicated in Fig. 33, the presence of low concentrations

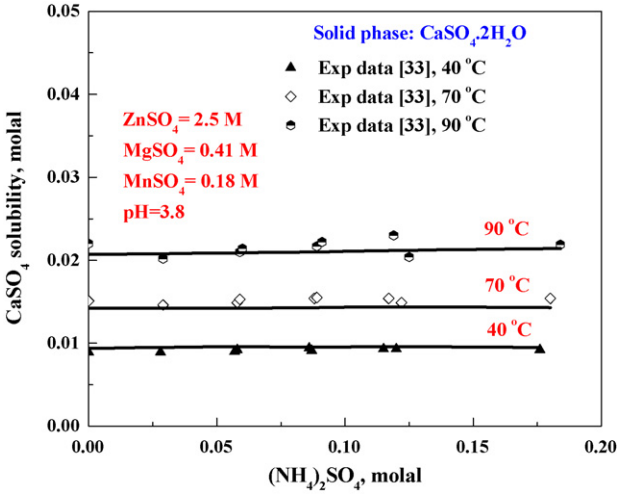

Fig. 33. $CaSO_4$ solubility in $CaSO_4$–$(NH_4)_2SO_4$–$ZnSO_4$ (2.5 M)–$MgSO_4$ (0.41 M)–$MnSO_4$ (0.18 M)–H_2SO_4 (pH 3.8)–H_2O solutions; the curves are the predicted values.

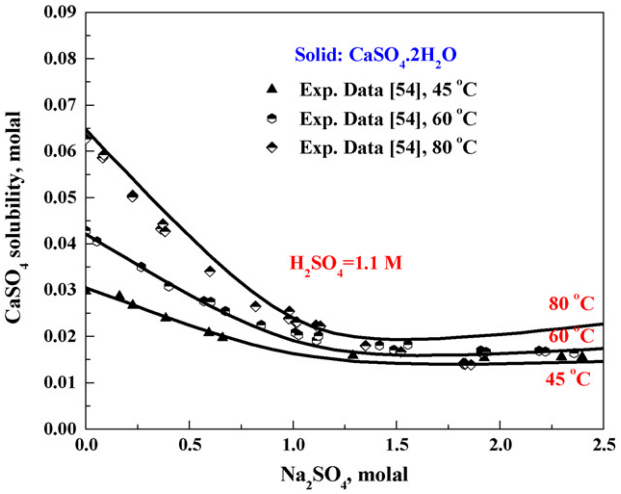

Fig. 34. $CaSO_4$ solubility in $CaSO_4$–Na_2SO_4–H_2SO_4 (1.1 M)–H_2O solutions at 45, 60 and 80 °C; the curves are the predicted values.

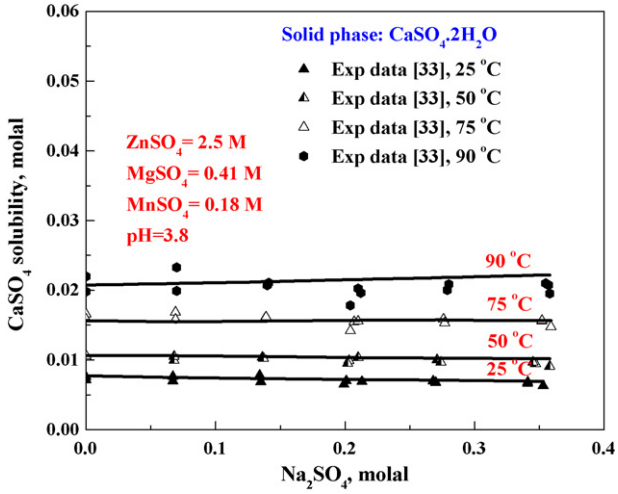

Fig. 35. $CaSO_4$ solubility in $CaSO_4$–Na_2SO_4–$ZnSO_4$ (2.5 M)–$MgSO_4$ (0.41 M)–$MnSO_4$ (0.18 M)–H_2SO_4 (pH 3.8)–H_2O solutions; the curves are the predicted values.

of NH_4^+ ion, as $(NH_4)_2SO_4$, has a minimal effect on the solubility of calcium sulphate; consequently, the ammonium additions required for the precipitation of jarosite-type compounds will have no significant effect on the solubility of calcium sulphate.

The experimental data and model prediction for this system are shown in Fig. 33, and the model prediction almost perfectly reflects the solubility of $CaSO_4$ in this multi-component acid-containing system.

3.3.7. $CaSO_4$–Na_2SO_4–H_2SO_4–H_2O system

The solubility of $CaSO_4$ in mixed Na_2SO_4 and H_2SO_4 aqueous solutions was measured by Kleinert and Wurm [54]. Fig. 34 shows the experimental $CaSO_4$ solubility versus Na_2SO_4 concentration in 1.1 mol/L H_2SO_4 solutions at three different temperatures. Even at the higher sulphuric acid concentrations, the new model very closely predicts the solubility of $CaSO_4$. Also, the trend shows that increasing sodium sulphate concentrations cause the solubility to decrease because of the formation of bisulphate (drop in acidity).

3.3.8. $CaSO_4$–Na_2SO_4–$ZnSO_4$ (2.5 M)–$MgSO_4$ (0.41 M)–$MnSO_4$ (0.18 M)–H_2SO_4 (pH 3.8)–H_2O system

As was discussed earlier, Na^+ ions are sometimes added to hydrometallurgical zinc operations in order to precipitate $Fe_2(SO_4)_3$ as a jarosite-type compound, and these ions will form aqueous Na_2SO_4. Therefore, the influence of sodium sulphate on the solubility of $CaSO_4$ is of some commercial relevance.

Dutrizac [33] measured the solubility of $CaSO_4$ versus the concentration of Na_2SO_4 in multi-component solutions containing $ZnSO_4$, $MgSO_4$, $MnSO_4$ and H_2SO_4. It was shown that increasing the Na concentration from 0 to 12 g/L has only a small effect on the solubility of $CaSO_4$, which decreases very slightly with increasing amounts of sodium sulphate. Generally, hydrometallurgical Zn processing solutions contain 1–5 g/L Na, and such concentrations will have a negligible effect on the solubility of $CaSO_4$ [33].

The experimental data and the model predictions are shown in Fig. 35, in which the model shows a near-perfect prediction of the solution chemistry.

4. Conclusions

It is clear that accurate solubility modelling is important to define the behaviour of calcium sulphate in aqueous solutions, and to assess the potential for scaling in various aqueous streams, especially for those systems where experimental data are lacking. To this end, the chemistry of several calcium sulphate systems was successfully modelled using the MSE (H_3O^+) model. The modelling involved the fitting of binary activity, heat capacity and solubility data, as well as ternary solubility data. New interaction parameters for free calcium ions and associated calcium sulphate neutral species with other dominant species in the solution were determined.

The model was shown to accurately predict the solubility behaviour of calcium sulphate in simulated zinc sulphate processing solutions containing $MgSO_4$, $MnSO_4$, $Fe_2(SO_4)_3$, Na_2SO_4, $(NH_4)_2SO_4$ and H_2SO_4, from room temperature to 95 °C. The solubility of calcium sulphate in water reaches a maximum around 40 °C, followed by a slight decrease of the solubility at higher temperatures. The addition of H_2SO_4 results in a significant increase in the calcium sulphate solubility. By increasing the acid concentration, gypsum which is the equilibrium saturating solid phase below 40 °C, dehydrates to anhydrite, and the conversion results in a decrease in the solubility of calcium sulphate. It was revealed that, in $ZnSO_4$-H_2SO_4 media, increasing $MgSO_4$, Na_2SO_4, $Fe_2(SO_4)_3$ and $(NH_4)_2SO_4$ concentrations do not have a significant effect on the solubility of calcium sulphate. As it is not practical to measure solubility data under all possible conditions, because of the large number of components involved, chemical modelling becomes a valuable tool for assessing the solubility of calcium sulphate for a wide variety of complex aqueous processing streams.

List of symbols

a	activity
a_i ($i = 1, \ldots, 4$)	*HKF* parameters
B_{ij}	binary interaction parameters between species i and j
BMDi	MSE adjustable parameters between species i and j
CMDi	MSE adjustable parameters between species i and j
c_i ($i = 1, 2$)	*HKF* parameters
C_p	heat capacity
CPS_i	heat capacity parameters of the solid
G^{E}	excess Gibbs free energy
GRES	standard state Gibbs free energy of the solid
ΔG°	Gibbs free energy of the reaction
H	enthalpy
I	ionic strength
K_{sp}	solubility product
$K_{\mathrm{T,P}}$	equilibrium constant
m	molality (mol/kg of water)
M	molarity (mol/L)
n_i	number of moles of species i
R	gas constant (8.314 J mol^{-1} K^{-1})
S	entropy
SRES	standard state entropy of the solid
V	volume
x_i	mole fraction of species i

Greek letters

γ_i	activity coefficient of species i
$\gamma_\pm$	mean activity coefficient of the electrolyte
μ_i^0	standard state chemical potential of species i
ν_i	stoichiometric coefficient
$\bar{\omega}$	HKF parameter

Subscripts

aq	aqueous
g	gaseous phase
LR	long-range interactions
MR	middle-range interactions
s	solid phase
SR	short-range interactions

Acknowledgements

The authors would like to acknowledge the financial support provided by Inco Technical Services Ltd., and the Natural Sciences and Engineering Research Council of Canada (NSERC) for this project.

Appendix A. MSE middle range ion interaction parameters (OLI-version 7.0.41)

System	Species i	Species j	BMD0	BMD1	BMD2	CMD0	CMD1	CMD2	Temperature range (°C)
$MnSO_4$–H_2O	Mn^{2+}	SO_4^{2-}	−716.1573	0.905887	93031.75	255.5114	–	–	0–180
$NiSO_4$–H_2O	Ni^{2+}	SO_4^{2-}	−62.8198	0.131417	−10727.55	29.0948	0.0107966	32862.21	0–300
$CaSO_4$–$(NH_4)_2SO_4$–H_2O	Ca^{2+}	NH_4^+	32.87928	−0.040706	–	−24.1034	–	–	25–100
	$CaSO_{4(aq)}$	NH_4^+	−28.30143	0.094104	–	–	–	–	
$Fe_2(SO_4)_3$–H_2SO_4–H_2O	Fe^{3+}	HSO_4^-	−199.0842	0.326877	21228.28	−51.03164	0.122383	–	25–140
$CaSO_4$–$MnSO_4$–H_2O	Ca^{2+}	Mn^{2+}	683.4903	−2.000546	–	−868.8426	2.517280	–	25–100
	$CaSO_{4(aq)}$	Mn^{2+}	2134.468	−2.830570	−394937.6	–	–	–	
$CaSO_4$–$MgSO_4$–H_2O	Ca^{2+}	Mg^{2+}	−277.3953	0.963089	–	387.3446	−1.350024	–	25–175
	$CaSO_{4(aq)}$	Mg^{2+}	−124.2653	0.339870	–	–	–	–	
$CaSO_4$–Na_2SO_4–H_2O	Ca^{2+}	Na^+	25.17114	−0.026235	–	−33.18963	0.021033	–	25–300
$MnSO_4$–H_2SO_4–H_2O	Mn^{2+}	HSO_4^-	−119.1324	0.271225	3062.835	741.6080	−1.254567	−105173.0	25–65
	$MnSO_{4(aq)}$	HSO_4-	−95.1999	–	–	121.8851	–	–	
$CaSO_4$–H_2SO_4–H_2O	Ca^{2+}	HSO_4-	−139.2929	0.126447	−5876.88	138.7389	–	–	25–300
$CaSO_4$–$ZnSO_4$–H_2O	Ca^{2+}	Zn^{2+}	−1483.251	2.251317	261185.4	966.7200	−1.646337	−168476.4	25–200
	$CaSO_{4(aq)}$	Zn^{2+}	−7553.179	11.22422	1245946.0	12259.72	−17.93268	2054992.0	
$CaSO_4$–$NiSO_4$–H_2O	Ca^{2+}	Ni^{2+}	−1201.110	2.268610	162651.9	288.3672	−1.053952	–	25–90
$CaSO_4$–$Fe_2(SO_4)_3$–$ZnSO_4$–H_2SO_4–H_2O	Ca^{2+}	Fe^{3+}	−4405.636	6.894359	732618.6	−113.2800	–	–	25–90
	$CaSO_{4(aq)}$	Fe^{3+}	463.0910	−0.597773	−84289.36	–	–	–	

Appendix B. The standard state Gibbs free energy, entropy and coefficients of heat capacity of the solid based on C_p = CPS1 + CPS2 × T + (CPS3/T^2) + CPS4 × T^2 + CPS5 × T^3 equation (OLI-version 7.0.41)

Reaction	G^0_{ref}	S^0_{ref}	CPS1	CPS2	Temperature range (°C)
$CaSO_4{\cdot}0.5H_2O = Ca^{2+} + SO_4{}^{2-} + 0.5H_2O$	−343902.4	31.47919	−188.165	0.9282105	0–200
$NiSO_4{\cdot}7H_2O = Ni^{2+} + SO_4{}^{2-} + 7H_2O$	−588710.4	93.10182	–	–	0–32
$NiSO_4{\cdot}6H_2O = Ni^{2+} + SO_4{}^{2-} + 6H_2O$	−531926.5	80.78579	–	–	32–100
$NiSO_4{\cdot}1H_2O = Ni^{2+} + SO_4{}^{2-} + 1H_2O$	−245961.9	21.08627	–	–	100–220
$MnSO_4{\cdot}7H_2O = Mn^{2+} + SO_4{}^{2-} + 7H_2O$	−632453.0	114.6626	682.6903	0.3383515	0–10
$MnSO_4{\cdot}5H_2O = Mn^{2+} + SO_4{}^{2-} + 5H_2O$	−518996.6	81.76251	368.0625	–	10–25
$MnSO_4{\cdot}1H_2O = Mn^{2+} + SO_4{}^{2-} + 1H_2O$	−291985.0	22.13603	−2206.528	7.682886	25–180

References

[1] J.F. Adams, Ph.D. Thesis, University of Toronto, Toronto, 2004.
[2] W.L. Marshall, R. Slusher, J. Phys. Chem. 70 (12) (1966) 4015–4027.
[3] K.K. Tanji, L.D. Doneen, Water Resour. Res. 2 (3) (1966) 543–548.
[4] J.F. Zemaitis, D.M. Clark, M. Rafal, N.C. Scrivner, Handbook of Aqueous Electrolyte Thermodynamics, DIPPR, AIChE, New York, 1986.
[5] G.P. Demopoulos, P. Kondos, V.G. Papangelakis, in: G.L. Strathdee, M.O. Klein, L.A. Melis (Eds.), Crystallization and Precipitation, Pergamon Press, Oxford, 1987, pp. 231–246.
[6] A. Arslan, G.R. Dutt, Soil Sci. 155 (1) (1993) 37–47.
[7] P. Wang, A. Anderko, R.D. Young, Fluid Phase Equilib. 203 (2002) 141–176.
[8] P. Wang, R.D. Springer, A. Anderko, R.D. Young, Fluid Phase Equilib. 222–223 (2004) 11–17.
[9] P. Wang, A. Anderko, R.D. Springer, R.D. Young, J. Mol. Liq. 125 (2006) 37–44.
[10] Z. Li, G.P. Demopoulos, Ind. Eng. Chem. Res. 45 (9) (2006) 2914–2922.
[11] Aqueous System Modelling Course and Workshop, OLI's Manual, OLI System Inc., New Jersey, 2002.
[12] H. Liu, V.G. Papangelakis, J.F. Adams, in: D.G. Dixon, M.J. Dry (Eds.), Computational Analysis in Hydrometallurgy, Canadian Institute of Mining, Metallurgy and Petroleum, Montreal, 2005, pp. 275–293.
[13] J.C. Tanger IV, H.C. Helgeson, Am. J. Sci. 288 (1988) 19–98.
[14] H. Liu, V.G. Papangelakis, Ind. Eng. Chem. Res. 45 (2006) 39–47.
[15] M. El Guendouzi, A. Mounir, A. Dinane, J. Chem. Thermodyn. 35 (2003) 209–220.
[16] G.G. Aseyev, Thermal Properties of Electrolyte Solutions. Methods for Calculation of Multi-component Systems and Experimental Data, Begell House Inc Publishers, New York. Wallingford, United Kingdom, 1996.
[17] W.F. Linke, A. Seidell, Solubilities of Inorganic and Metal-organic Compounds, American Chemical Society, Washington, DC, vol. I: 1958, vol. II: 1965.
[18] H.P. Snipes, C. Manly, D.D. Ensor, J. Chem. Eng. Data 20 (3) (1975) 287–291.
[19] H. Yokoyama, H. Yamatera, Bull. Chem. Soc. Japan 48 (10) (1975) 2708–2718.
[20] H.F. Holmes, R.E. Mesmer, J. Chem. Thermodyn. 18 (3) (1986) 263–275.
[21] J.A. Rard, D.G. Miller, J. Chem. Eng. Data 26 (1) (1981) 33–38.
[22] J.K. Hovey, K.S. Pitzer, J.A. Rard, J. Chem. Thermodyn. 25 (1) (1993) 173–192.
[23] W.C. Schroeder, A. Gabriel, E.P. Partridge, J. Am. Chem. Soc. 57 (9) (1935) 1539–1546.
[24] R.A. Robinson, R.H. Stokes, Electrolyte Solutions, second revised edition, Dover Publications Inc., New York, NY, 2002.
[25] W.W. Rudolph, J. Solution Chem. 28 (1999) 621–630.
[26] G. Bruhn, J. Gerlach, F. Pawlek, Z. Anorg. Allgem. 337 (1–2) (1965) 68–79.
[27] G.A. Hulett, L.E. Allen, J. Am. Chem. Soc. 24 (1902) 667–679.
[28] A.E. Hill, N.S. Yanick, J. Am. Chem. Soc. 57 (1935) 645–651.
[29] A.E. Hill, J.H. Wills, J. Am. Chem. Soc. 60 (1938) 1647–1655.
[30] E. Posnjak, Am. J. Sci. 35A (1938) 247–272.
[31] W.L. Marshall, R. Slusher, E.V. Jones, J. Chem. Eng. Data 9 (2) (1964) 187–191.
[32] W.L. Marshall, E.V. Jones, J. Phys. Chem. 70 (1966) 4028–4040.
[33] J.E. Dutrizac, Hydrometallurgy 65 (2–3) (2002) 109–135.
[34] E.P. Partridge, A.H. White, J. Am. Chem. Soc. 51 (2) (1929) 360–370.
[35] U. Sborgi, C. Bianchi, Gazzetta Chemica Italiana 70 (1940) 823–835.
[36] F.G. Straub, Ind. Eng. Chem. 24 (8) (1932) 914–917.
[37] Y. Ling, G.P. Demopoulos, J. Chem. Eng. Data 49 (2004) 1263–1268.
[38] A.B. Zdanovskii, G.A. Vlasov, Russ. J. Inorg. Chem. 13 (9) (1968) 1318–1319.
[39] A.B. Zdanovskii, G.A. Vlasov, L.I. Sotnikova, Russ. J. Inorg. Chem. 13 (1968) 1418–1420.
[40] Y. Umetsu, B.K. Mutalala, K. Tozawa, J. Mining Metallurgy Japan 6 (1989) 13–22.
[41] K.K. Tanji, Environ. Sci. Technol. 3 (7) (1969) 656–661.
[42] L.V. Novikova, Russ. J. Inorg. Chem. 2 (3) (1957) 300–312.
[43] V.M. Zatonskaya, N.A. Volkova, S.V. Krashenina, A.I. Samoilenko, N.F. Burtseva, Tsvetnye Metally (Non-Ferrous Metals) 29 (2) (1988) 25–26.
[44] G. Supatashvili, N. Takaishvili, G. Macharadze, Bull. Georgian Acad. Sci. 155 (1) (1997) 68–71.
[45] J. Block Jr., O.B. Waters, J. Chem. Eng. Data 13 (3) (1968) 336–344.
[46] C.C. Templeton, J.C. Rodgers, J. Chem. Eng. Data 12 (4) (1967) 536–547.
[47] W.L. Denman, Ind. Eng. Chem. 53 (10) (1961) 817–822.
[48] H.L. Silcock, Solubilities of Inorganic and Organic Compounds, vol. 3, Pergamon Press, New York, NY, 1979.
[49] B.I. Zhelnin, G.I. Gorshtein, L.Kh. Bezprozvannaya, J. Appl. Chem. USSR 46 (3) (1973) 534–537 (English translation).
[50] A.N. Campbell, N.S. Yanick, Trans. Faraday Soc. 28 (1932) 657–661.
[51] W.H. Baskerville, F.K. Cameron, J. Phys. Chem. 39 (6) (1935) 769–779.
[52] E. Posnjak, H.E. Merwin, J. Am. Chem. Soc. 44 (9) (1922) 1965–1994.
[53] F. Wirth, B. Bakke, Z. Anorg. Chem. 87 (1) (1914) 13–46.
[54] T. Kleinert, P. Wurm, Monatshefte fuer Chemie 83 (1952) 459–462.
[55] G.N. Kononova, B.A. Redzhepov, Russ. J. Inorg. Chem. 41 (7) (1996) 1173–1177.